4-2023

Metabolomic differentiation of tumor core and edge in glioma.

Mary E. Baxter
University of Louisville

METABOLOMIC DIFFERENTIATION OF TUMOR CORE AND EDGE IN GLIOMA

By

Mary Elizabeth Baxter

B.S., University of Louisville, 2022

A Thesis

Submitted to the Faculty of the

J.B. Speed School of Engineering of the University of Louisville

In Partial Fulfillment of the Requirements

for the Degree of

Master of Science in Bioengineering

Department of Bioengineering

University of Louisville

Louisville, Kentucky

May 2023

METABOLOMIC DIFFERENTIATION OF TUMOR CORE AND EDGE IN GLIOMA

Submitted by

Mary E. Baxter

A Thesis Approved on

17 April 2023

By the Following Reading and Examination Committee:

Hermann Frieboes Digitally signed by Hermann Frieboes Date: 2023.04.17 19:13:35 -04'00'

Thesis Chair

Nihat Altiparmak Digitally signed by Nihat Altiparmak Date: 2023.04.18 22:34:08 -04'00'

Committee Member

Joseph Chen Digitally signed by Joseph Chen Date: 2023.04.18 22:45:40 -04'00'

ACKNOWLEDGEMENTS

I humbly thank my technical mentor, Dr. Hunter Miller, for his generous guidance and kind patience. This work would not have been possible without him. I also want to extend gratitude to my primary investigator, Dr. Hermann Frieboes, for the opportunity to contribute to the work of his lab and his continued support throughout my undergraduate and graduate years.

I thank Dr. Brian Williams, for providing the clinical samples for our analysis and helping to identify key points of investigation; Dr. Joseph Chen, for helping to formulate the hypothesis of our study and serving on the committee; Dr. Nihat Altiparmak, for his support and service on the committee; Melissa Hall and Danyelle Clark, for their help to access up-to-date patient information from the James Graham Brown Cancer Center; and University of Louisville Center for Regulatory and Environmental Analytical Metabolomics, for processing our samples and identifying metabolites via liquid chromatography and mass spectrometry.

I would also like to thank Bioengineering doctoral candidate Dylan Goodin, for his consistent encouragement. His spirit consistently motivated me. In addition, I thank Bioengineering undergraduate students Sarah Lee and Liam Hurley, for their academic support and friendship; and my parents, siblings, and grandparents, for their generous moral support.

ABSTRACT

Glioma is one of the most aggressive forms of brain cancer. It has been shown that the microenvironments differ significantly between the core and edge regions of glioma tumors. This study obtained metabolomic profiles of glioma core and edge regions using paired glioma core and edge tissue samples from 27 human patients. Data was acquired by performing liquid-liquid metabolite extraction and 2DLC-MS/MS on the tissue samples. In addition, a boosted generalized linear machine learning model was employed to predict the metabolomic profiles associated with O-6-methylguanine-DNA methyltransferase (MGMT) promoter methylation.

A panel of 66 metabolites was found to be statistically significant between the core and edge regions. The machine learning model achieved AUROC values of 0.941 for the core and 0.960 for edge. This proof-of-concept study shows the metabolomic differences are reflected in MGMT promoter methylation status and demonstrates the potential for machine learning to aid as a prognostic and therapeutic tool.

TABLE OF CONTENTS

LIST OF FIGURES

OBJECTIVES

Gliomas exhibit high intra-tumor and inter-patient heterogeneity. Recently, it has been shown that the microenvironment and phenotype differ significantly between glioma core (inner) and edge (infiltrating) regions. This proof-of-concept study differentiates metabolic signatures associated with these regions, with the potential for prognosis and targeted therapy that could improve surgical outcomes.

METHODS SUMMARY

Paired glioma core and infiltrating edge samples were obtained from 27 human patients after craniotomy. Liquid-liquid metabolite extraction was performed on the samples and metabolomic data was obtained via 2DLC-MS/MS. To gauge the potential of metabolomics to identify clinically relevant predictors of survival from tumor core vs. edge tissues, a boosted generalized linear machine learning model was employed to predict metabolomic profiles associated with O-6-methylguanine-DNA methyltransferase (MGMT) promoter methylation.

RESULTS SUMMARY

A panel of 66 (out of 168) metabolites was found to significantly differ between glioma core and edge regions ($p \leq 0.05$). Top metabolites with significantly different relative abundances included DL-alanine, creatine, cystathionine, nicotinamide and D-pantothenic acid. Significant metabolic pathways identified by QEA analysis included glycerophospholipid metabolism, butanoate metabolism, cysteine and methionine metabolism, glycine, serine, alanine and threonine metabolism, purine metabolism, nicotinate and nicotinamide metabolism, and pantothenate and CoA biosynthesis. The machine learning model using four key metabolites each within core and edge tissue specimens predicted MGMT promoter methylation status with $AUROC_{Edge} = 0.960$ and $AUROC_{Core} = 0.941$. Top metabolites associated with MGMT status in core included hydroxyhexanoycarnitine, spermine, succinic anhydride, and pantothenic acid, and in edge included 5-CMP, pantothenic acid, itaconic acid, and uridine.

CONCLUSIONS SUMMARY

Key metabolic differences are identified between core and edge tissue in glioma and, further, demonstrate the potential for machine learning to provide insight into potential prognostic and therapeutic targets.

INTRODUCTION

Tumor heterogeneity in glioblastoma (GBM) can be described by two major regions, the core (inner) and edge (infiltrating), which harbor unique environments[1,2] that underlie the progression of GBM and are associated with pro-malignant processes including phenotypic transitions and heightened invasiveness, respectively. Recent work has also suggested that metabolic changes manifest spatially across the tumor and are essential mediators of tumor adaptation and therapy evasion. The edge demonstrates an increased expression of genes associated with fatty acid metabolism as well as abundance of acylcarnitines, but also has high glucose metabolism[1], while the core tends to exhibit more metabolic plasticity and reliance on amino acid metabolism[3]. Although the contributions of metabolic changes to GBM progression are clear, the specific metabolites and metabolic pathways responsible for these alterations are poorly understood.

Metabolomics provides a potential advantage in its ability to describe functional changes to the cells that complement the transcriptional and proteomic profiles of the tumor[4 5]. Early reports in metabolomics studies have shown that unique metabolic signatures can be identified between low grade and high-grade gliomas via tissue and serum from patients[6]. One study that performed GC/MS with cerebrospinal fluid (CSF) found citric and isocitric acid to have higher abundances in GBM than in grades I-III gliomas[7]. Metabolomics studies have traditionally utilized human body fluids such as urine, blood, CSF, and other sera to characterize cancer[7]. However, these approaches cannot resolve differences within the tumor. Therefore, studying the cancer tissue directly, rather than the biofluids, may provide more accurate insight into intra-tumoral metabolic

differences[8], and yield detailed information about tumor microenvironment heterogeneity and potential cell-scale mechanisms[9]. Very recently, key metabolic differences between adult glioma subtypes were identified from resected tissue[10].

A variety of techniques have been applied for analysis of metabolomic data, including network-oriented techniques, such as principal network analysis, and data-driven methods, such as statistical modeling and machine learning[11], as recently reviewed[12]. In parallel, substantial work has focused on application of machine learning to GBM imaging data, including radiomics and radiogenomics[13,14], for detecting true progression from pseudoprogression[15], to evaluate intra-tumoral heterogeneity[16,17],and to analyze MRI with deep learning[18,19]. In this study, core and edge GBM tumor tissue pairs obtained from craniotomy and resection underwent liquid-liquid metabolite extraction, and the metabolomic profiles of the core and edge regions were contrasted. Differences in these profiles are important because the core is typically removed through surgery while the edge is left behind. Further, machine learning was applied to evaluate the potential of metabolomics to identify clinically relevant predictors of survival from tumor core vs. edge tissues. Here, O-6-methylguanine-DNA methyltransferase (MGMT) promoter methylation was chosen as an example for evaluation, with the goal to demonstrate the capability to provide insight into potential prognostic and therapeutic targets. MGMT promoter methylation status has been associated with GBM patient prognosis, where methylation typically improves overall survival[20]. The MGMT promoter is a DNA repair protein and is associated with alkylating chemotherapeutic agents, such as TMZ[21,22]. It is currently unknown how MGMT promoter methylation status manifests in the metabolome of GBM tissue. Applying machine learning to deepen the understanding of GBM intra-tissue

metabolomic heterogeneity and identifying key differences would be relevant for future customization of treatment.

METHODS

Patient sample tissue and gene status collection

Informed consent was obtained to participate in this study. All specimens were collected following approved Internal Review Board protocols at University of Louisville Hospital (IRB 20.0219) from patients with known or suspected brain tumors. As brain cancer affects both women and men, samples from both were collected. Samples were collected by the clinical team, blinded to the research analysis. Patient information was de-identified by the clinical team before evaluation by the research team. IDH-R132H mutation was detected by immunohistochemistry and MGMT promotor methylation by next generation sequencing (Neogenomics Inc., Fort Meyers, FL).

Patient sample tissue processing for metabolomics

Samples of 27 GBM tumor core and edge pairs were received from the University of Louisville Brown Cancer Center Biorepository at separate times from human patients immediately following craniotomy, for a total of 54 samples. Core samples were collected from the contrast enhancing portion of the tumor (**Figure_1**). Infiltrating edge samples were collected from T2/FLAIR hyperintense surrounding tissue (**Figure_2**). For each core-edge pair following craniotomy, the two sections were immediately placed into separate 15mL centrifuge tubes containing 5mL non-supplemented RPMI medium and transferred to the lab for processing. Tissue sections were placed in separate sterile 1.5mL microcentrifuge tubes with tweezers. All tissue handling was performed under biosafety cabinet in sterile environment. PBS (1mL) was added to each tube, and tubes were

centrifuged 250xg for 5min. After supernatant was aspirated, this washing step was repeated for both samples. 500µL cold acetonitrile was added to each sample after second supernatant was aspirated; samples were then homogenized with handheld pellet mixer (VWR 47747-370) by grinding the sample against microcentrifuge tube wall. Next, 375µL nuclease-free water and 250µL chloroform were added to each tube, followed by vortexing 10-15 sec. A final 20min centrifugation 664xg was completed to separate polar, protein, and lipid layers. Polar and lipid layers were pipetted for each sample into 1.5mL microcentrifuge tubes and 2.0mL glass screw top vials, respectively, and polar layers were lyophilized.

2DLC-MS/MS Sample Processing

Post-lyophilization, 2DLC-MS/MS was performed by the Center for Regulatory and Environmental Analytical Metabolomics (CREAM) at the University of Louisville. Each dried sample was dissolved in 200µL 50% acetonitrile and vigorously vortexed 3min. After centrifugation 14,000rpm and 4^{o}C for 20min, 100µL was collected for further analysis. All samples were analyzed on Thermo Q Exactive HF Hybrid Quadrupole-Orbitrap Mass Spectrometer coupled with Thermo DIONEX UltiMate 3000 HPLC system (Thermo Fisher Scientific, Waltham, MA). The LC system is equipped with reversed phase column (RPC, Waters Acquity UPLC HSS T3 column, 2.1x150mm, 1.8µm) and hydrophilic interaction chromatography column (HILIC, Millipore SeQuant ZIC-cHILIC column, 2.1x150mm, 3µm). The two chromatographic columns were configured to form a parallel 2DLC-MS system [9]. Mobile phase_A was water with 0.1% formic acid for PRC and 35% acetonitrile with 10mM ammonium acetate (pH adjusted to 3.25 with acetate) for HILIC. Mobile phase_B was acetonitrile with 0.1% formic acid for both RPC and HILIC. RPC gradient was 0% B, hold for 6.0min; 6.0 to 14min, 0% B to 28% B; 14.1 to 16min,

28% B to 50% B; 16.1 to 20.0min, 50% B to 100% B, hold for 1.0min; 21 to 21.1min, 100% B to 0% B, hold for 11.9min. The HILIC gradient was 0 to 1.3min, 95% B; 1.3 to 8.3min, 95% B to 0% B, hold for 2.7min; 11.0 to 11.5min, 0% B to 95% B, hold for 11.5min. Flow rate was 0.35mL/min for RPC or 0.3mL/min for HILIC. Column temperature was 40°C for both RPC and HILIC. Samples were first analyzed in a random order in positive (+) and negative (-) modes to obtain full MS data for metabolite quantification. For metabolite identification, a pooled sample of each group was analyzed by 2DLC-MS/MS in positive and negative modes at three collision energies, 20, 40, and 60eV.

2DLC-MS/MS Data Analysis

(XCMS, RRID:SCR_015538, xcmsonline.scripps.edu) was used for spectrum deconvolution[23], and MetSign software for metabolite identification, cross-sample peak list alignment, normalization, and statistical analysis[24,25]. To identify metabolites, 2DLC-MS/MS data was first matched to an in-house database that contains parent ion m/z, MS/MS spectra, and retention time of authentic standards. Threshold for spectral similarity was set ≥0.4, while thresholds of retention time difference and m/z variation window were respectively set ≤0.15min and ≤5 ppm. 2DLC-MS/MS data without a match with the metabolites in the in-house database were further analyzed using Compound Discoverer software (v2.0, Thermo Fisher Scientific, Germany), where MS/MS spectra similarity score threshold was set ≥40 with a maximum score of 100. This analysis yielded the intensity peaks for individual metabolites identified in each sample.

Data Pre-Processing

Data pre-processing was performed using R programming Language v.4.1.0. The metabolite intensity peaks from 2DLC-MS/MS were imported from an Excel file.

Metabolites absent in 30% or more of the samples were excluded, resulting in 168 unique metabolomic signatures detected across all analytical batches (**Supplementary_Figure_1**). Data was pre-processed by log transformation and mass spectrometry total useful signal (MSTUS) normalization, both commonly used in metabolomics[5,26], and centering. The log transform was applied to minimize heteroscedasticity[5]. MSTUS normalization, especially used for liquid chromatography, sums ion MS signals that are common among all samples to develop a normalization factor[26]. Data was centered around the mean to focus on the differences between the data[5]. Since data appeared to be missing at random (**Supplementary_Figure_1**), imputation was performed to handle missing values by Bayesian Principal Component Analysis (BPCA). Data from all 27 patients were obtained across two separate analytical batches. Batch correction was performed by the *ber* statistical model[27] on positive and negative ion mode datasets separately (**Supplementary_Figure_2**).

Statistical Analyses

Paired and unpaired statistical analyses were performed in R v.4.1.0. Shapiro test was used to determine normality; t-test or Wilcoxon-rank sum test (Mann-Whitney U test) was used to determine significant differences between relative abundance of metabolites. A Partial Least Squares Discriminant Analysis (PLS-DA) analysis was performed with function *plsda* from *mdatools* library. Heat map of pre-processed data was generated with *heatmap.2* function from *gplots* library.

Classification Model

A machine learning model (glmboost) was trained to discriminate between MGMT promoter methylation positive and negative samples using tumor core and edge

metabolomic data independently. A rigorous combination of feature selection and cross validation was performed to prevent overfitting. Test set validation was achieved with 5-fold cross-validation, performed with 20 iterations of random subsampling. Results were obtained as the average across all folds and iterations. Classification performance metrics (AUROC; F1) were calculated as the averages across all folds and resampling iterations. Forward feature selection was performed after ranking features by variable importance and training/validating models on feature subsets 2 through 16. Across all feature subsets, a single optimal trained model was identified for the tumor core and edge. Variable importance was calculated as the absolute value of the coefficients of the tuned model, using function *varImp* from package *caret*. Model hyperparameters *mstop* (number of boosting iterations) and *prune* (AIC prune boolean) were tuned with R package *caret* (version 6.0-93), where prune="no" and mstop=450 and 150 for models trained with core and edge data, respectively.

Metabolic Network Visualization and Quantitative Enrichment Analysis

(MetaboAnalyst 5.0, RRID:SCR_015539, www.metaboanalyst.ca/)[28] was used to obtain chemical structure classes and quantitative enrichment analysis (QEA). (KEGG, RRID:SCR_012773, www.kegg.jp/) database was accessed (March 2023). Metabolic networks were visualized with (Cytoscape 3.8.2, RRID:SCR_003032, cytoscape.org/) and (MetScape 3.1.3, RRID:SCR_014687, metscape.ncibi.org/).

RESULTS

Patient characteristics

Of 27 patients (**Table_1**), 23 were white and 4 were of Black or African American ethnicity. Average age at tissue collection was 52 years (±17.7). Twenty-two patients had WHO grade 4 GBM; remainder was of astrocytoma, oligoastrocytoma or oligodendroglioma histology. All patients had *IDH1* mutation status, with 6 positive; of 22 patients with MGMT promoter methylation status, 7 were positive.

Metabolic differences in tumor core and edge tissue

PLS-DA separated tumor core and edge samples significantly ($P_{overlap}$ = 5.37E-11) (**Figure_3**). A volcano plot of upregulated and downregulated metabolites between tumor core and edge is also shown. Metabolites with significant differences in relative abundance between paired tumor core and edge samples are in **Supplementary_Table_1**, with the top 20 (by lowest p-value) compared between core and edge in **Figure_4**. Top metabolites upregulated in edge were DL-alanine (p=6.41E-07), creatine (p=7.85E-07), cystathionine (p=1.02E-06), nicotinamide (p=1.31E-06), D-pantothenic acid (p=1.47E-06), and 3-Hydroxy-3-[(3-methylbutanoyl)oxy]-4-(trimethylammonio)butanoate (p=3.08E-06). Top metabolites upregulated in core were 2-oxobutyric acid, uric acid, threonine, and N1,N12-Diacetylspermine Comparison of remaining significant metabolites between core and edge are in **Supplementary_Figures_3-5**. Further, 5 metabolites were identified with significantly different relative abundance between patients with MGMT promoter methylation positive or negative status, including higher hydroxyhexanoycarnitine and

lower spermine in core, and both higher itaconic acid and pantothenic acid in edge (**Supplementary_Figure_6**, **Supplementary_Table_2**).

Classifying samples by MGMT promoter methylation status

PLS-DA score plots reveal significant separation between MGMT promoter methylation negative and positive samples using both tumor core ($P_{overlap}$ =3.18E-05) and edge ($P_{overlap}$ =3.11E-04) metabolomic data (**Figure_5**). This indicates that classification via machine learning could provide insight. A classification model was trained and validated as described in **Figure_6**. Excellent classification performance (**Figure_5C)** was achieved using the top 4 metabolomic features as ranked by variable importance (**Supplementary_Table_3**), with AUROC $_{Core}$ = 0.941 (0.905 - 0.967) (95%CI) and AUROC $_{Edge}$ =0.960 (0.937 - 0.982) (95%CI). Model performance across all feature subsets (2-10 or 2-11 for edge and core, respectively) is summarized in **Supplementary_Figure_7.** For both the tumor core and edge, AUROC increases initially and begins to decline after 4 features, while F1 also shows a decline after 4 features. Overall, these results indicate that the features ranked by glmboost variable importance were effective at filtering noise out of the datasets.

Quantitative enrichment analysis

The relative proportion of chemical structure main classes within tumor core and edge samples across both analytical batches is in **Supplementary_Figure_8**. Largest classes included amino acids and peptides, fatty acids and conjugates, fatty esters, pyrimidines, purines and TCA acids. The most significantly enriched metabolic pathways between core and edge (**Supplementary_Figure_9**), where the enrichment ratio is the number of observed hits divided by the number of expected hits, were glycine, serine and

threonine metabolism; nicotinate and nicotinamide metabolism; pantothenate and CoA metabolism; glutathione metabolism; cysteine and methionine metabolism. Pathway maps of significant metabolic pathways identified by QEA analysis for tumor core vs. edge are in **Figure_7** and **Supplementary_Figure_10**.

DISCUSSION

Little is known about differences in metabolic landscapes in spatially distinct core and edge (infiltrating) regions of gliomas. This proof-of-concept study identified 66 unique metabolomic signatures that differed significantly between paired core and edge human glioma specimens (**Figure_3**). A total of 5 metabolites were found to be significantly different in terms of relative abundance each between MGMT promoter methylation positive and negative patients (**Supplementary_Figure_6**). Further, a machine learning model (glmboost) was able to accurately classify MGMT promoter methylation status using metabolomic data from tumor core and edge (**Figure_5C**).

The tricarboxylic acid (TCA) cycle occurs within mitochondria in order to produce adenosine triphosphate (ATP)[29]. Glutamic acid, a significantly differentiated metabolite found between core and edge (**Supplementary_Figure_3**), , is referred to synonymously as glutamate (Glu), the form of glutamic acid found within the body[29]. Glu is highly involved in energy metabolism[29]. It is a key factor in glutaminolysis, a process that prepares substrates for the TCA cycle and serves an important role in cancer metabolism [29]. An increased level of Glu in the edge relative to the core, therefore, reflects the actively invasive nature of the edge. Astrocytes have been shown to uptake extra Glu produced by glioma cells[29]; however, if the astrocyte-to-glioma-cell ratio is too small, such as during higher grade glioma, when the ratio approximates 0.5:1, then cell death may ensue[29]. Glutamine, a driver of invasion in GBM, is abundant in the brain and is a direct precursor to Glu[30]. Glu is formed by a phosphate activated glutaminase, D-Glutamine

amidohydrolase, which also yields ammonia via reaction R01579 (KEGG) (**Figure_7**)[30]. Gliomas uptake glutamine through the upregulation of transporters of glutamine and Glu, and its deprivation is known to slow GBM tumor growth[31]. The results suggest that increased Glu detected in the infiltrating tumor edge may be due to increased glutamine uptake and conversion.

Furthermore, pyruvate (**Supplementary _Table _3**) as a TCA cycle intermediate is associated with increased levels of Glu, citrate, malate, and aspartate[32]. Creatine (**Figure_4**) , associated with amino-acid metabolism, has been noted as an energy metabolism marker[33]. It is unsurprising, therefore, that creatine and Glu were found to be upregulated in the edge (infiltrating) tumor regions. Pantothenic acid, also known as vitamin B5 and pantothenate, is an essential cofactor involved in many metabolic reactions and is the precursor of co-enzyme A (CoA)[34,35]. CoA is an essential component of acetyl-CoA, which serves many roles and participates in the TCA cycle and B-oxidation (lipid catabolism)[36]. D-Pantothenic acid, detected as a positive ion, was upregulated in tumor edge samples (**Figure_4**) and pantothenic acid, detected as a negative ion, was also included in the top 10 metabolites as ranked by the classification model using either tumor core or edge data (**Supplementary_Table_3**). Succinic anhydride, the acid anhydride of succinic acid, was also upregulated in tumor edge (**Supplementary_Figure_4**), consistent with the finding that succinate accumulation enables tumor cells to be more aggressive[37].

Uric acid (i.e. urate) was among the top 20 most significant metabolites in terms of relative abundance between core and edge tissue (**Figure_4**) and was also within the top 10 most important metabolites for predicting MGMT promoter methylation status using core tissue data (**Supplementary Table_3**). Uric acid levels may correlate with cancer

progression[38]. Deng et al. found that Type-II diabetes patients with higher levels of serum uric acid levels (≥5.0mg/dL) experienced significantly higher rates of cancer than those with lower levels (<3.0mg/dL)[38]. It remains unclear why uric acid levels would be increased in the core of gliomas. Nicotinamide, a form of vitamin B3, was the fourth most significantly upregulated metabolite in the infiltrating tumor edge (**Figure_4**) and nicotinate and nicotinamide metabolism was found to be the second most significantly enriched metabolic pathway (**Supplementary_Figure_9**). Nicotinamide has been associated with neuronal development, survival, and central nervous system (CNS) function, and has implications in neurodegenerative conditions such as Alzheimer's[39]. Nicotinamide N-methyltransferase is known to be overexpressed in GBM and is preferentially expressed by glioblastoma stem cells (GSCs)[40]. Nicotinamide is an important intermediate in the production of nicotinamide adenine dinucleotide (NAD+) and is involved with the maintenance of NAD and NADP[39]. Nicotinamide is connected with NAD+ directly via reactions R00555 and R00110 (KEGG) (**Supplementary_Figure_10**). NAD+ regulates functions for many metabolic pathways, including glycolysis and the TCA cycle[41]. Intracellular NAD(H) levels have been found to control motility and invasion in glioma cells, for which downregulation of NAMPT resulted in limited cell migration compared to controls[42]. Oral supplementation with nicotinamide has been shown to increase blood levels of NAD, suggesting that high levels of nicotinamide may increase the biosynthesis of NAD[43]. It can, therefore, be hypothesized that increased levels of nicotinamide in the infiltrating tumor edge found may also result in increased NAD levels, suggesting that NAD biosynthesis may reflect intratumoral heterogeneity. Higher NAD in

the tumor edge would further support the evidence that NAD levels have an impact on cell motility in glioma.

Purine metabolism (**Supplementary_Figure_10**), a pathway found to be significantly enriched between core and edge tissue, has recently garnered interest in the study of glioma metabolism[44,45]. It has been established that brain tumor initiating cells (BTICs) are dependent on the downstream components of *de novo* purine synthesis[45]. It is known that the GBM tumor edge has a preferential expression of glioma stem-like cell (GSC) signatures, where CD133 and CD109 have different expression profiles in tumor cells localized at the core and edge[46]. Hypoxanthine, which was increased in the tumor edge (**Supplementary_Figure_3**), has also been found to be elevated in BTICs[45]. Guanosine monophosphate (GMP), which is linked to hypoxanthine through inosine monophosphate (IMP) and reactions R01134 and R01132 (KEGG) (**Supplementary_Figure_10**), was also elevated in the tumor edge (**Supplementary_Figure_4**). GMP has been found to be essential to the maintenance of BTIC proliferation, self-renewal and tumorigenicity[45]. Taken together, these differences may indicate an increased abundance of this cell phenotype in the tumor edge. GMP was also found to be dramatically decreased in GBM tissue treated with Temozolomide (TMZ)[44]. Interestingly, uric acid (i.e. urate) was increased in the tumor core (**Figure_4**), which may indicate a decreased rate of production of uric acid in the tumor edge from hypoxanthine or xanthine through reactions R01768 and R02107 (KEGG) (**Supplementary_Figure_10**). The pathway analysis further highlights ethanolamine phosphate downregulated in core, indicating reduced lipid metabolism[47]; serine upregulated in core, promoting cell adaptation to hypoxic conditions[48]; decreased

cystathionine in core, linked to GBM progression[49]; methionine higher in core and known to be prevalent in glioma[50].

Due to the limited sample size in this proof-of-concept study, potential confounding variables age, histology, *IDH1* mutation, MGMT promoter methylation status, and primary vs. recurrent disease could not be adjusted for (**Table_1**). Accounting for these variables is planned in the future with a larger sample set. GBM is heterogeneous and consists of multiple cell types, including tumorigenic stem cells, stromal cells and differentiated bulk tumor cells[51,52]. The bulk tissue specimen analysis utilized in this study is useful for determining global characteristics of the broadly defined tissue regions, but more nuanced specimen analyses could be performed, e.g., via single cell matrix assisted laser desorption/ionization MS (MALDI MS)[53]. Moreover, platforms such as MetaboAnalyst are limited because not all metabolites have been documented in reference databases; thus, several compounds detected here could not be characterized or classified.

CONCLUSIONS

We have presented a proof-of-concept study evaluating metabolic differences in paired tumor core and infiltrating edge glioma samples and shown that unique metabolomic signatures distinguish these two tumor regions. Further, the potential of metabolomics to identify clinically relevant predictors of survival from these regions was evaluated by accurately classifying MGMT promoter methylation status. Longer term, metabolomics integrated with other analyses such as tumor tissue biophysical characterization might provide a comprehensive view of glioma heterogeneity. Investigation of mechanisms driving tumor aggression and invasion separately within core and edge could potentially identify therapeutic targets to minimize recurrence and benefit surgical outcomes.

REFERENCES

1. Randall EC, Lopez BGC, Peng S, et al. Localized Metabolomic Gradients in Patient-Derived Xenograft Models of Glioblastoma. *Cancer Res*. Mar 15 2020;80(6):1258-1267. doi:10.1158/0008-5472.CAN-19-0638

2. Lin CM, Yu CF, Huang HY, Chen FH, Hong JH, Chiang CS. Distinct Tumor Microenvironment at Tumor Edge as a Result of Astrocyte Activation Is Associated With Therapeutic Resistance for Brain Tumor. *Front Oncol*. 2019;9:307. doi:10.3389/fonc.2019.00307

3. Garcia JH, Jain S, Aghi MK. Metabolic Drivers of Invasion in Glioblastoma. *Front Cell Dev Biol*. 2021;9:683276. doi:10.3389/fcell.2021.683276

4. Griffin JL, Kauppinen RA. A metabolomics perspective of human brain tumours. *Febs j*. Mar 2007;274(5):1132-9. doi:10.1111/j.1742-4658.2007.05676.x

5. van den Berg RA, Hoefsloot HC, Westerhuis JA, Smilde AK, van der Werf MJ. Centering, scaling, and transformations: improving the biological information content of metabolomics data. *BMC Genomics*. Jun 8 2006;7:142. doi:10.1186/1471-2164-7-142

6. Marziali G, Signore M, Buccarelli M, et al. Metabolic/Proteomic Signature Defines Two Glioblastoma Subtypes With Different Clinical Outcome. *Sci Rep*. Feb 9 2016;6:21557. doi:10.1038/srep21557

7. Nakamizo S, Sasayama T, Shinohara M, et al. GC/MS-based metabolomic analysis of cerebrospinal fluid (CSF) from glioma patients. *J Neurooncol*. May 2013;113(1):65-74. doi:10.1007/s11060-013-1090-x

8. Miller HA, Yin X, Smith SA, et al. Evaluation of disease staging and chemotherapeutic response in non-small cell lung cancer from patient tumor-derived metabolomic data. *Lung Cancer*. 2021/06/01/ 2021;156:20-30. doi:https://doi.org/10.1016/j.lungcan.2021.04.012

9. Wang LB, Karpova A, Gritsenko MA, et al. Proteogenomic and metabolomic characterization of human glioblastoma. *Cancer Cell*. Apr 12 2021;39(4):509-528 e20. doi:10.1016/j.ccell.2021.01.006

10. Bjorkblom B, Wibom C, Eriksson M, et al. Distinct metabolic hallmarks of WHO classified adult glioma subtypes. *Neuro Oncol*. Sep 1 2022;24(9):1454-1468. doi:10.1093/neuonc/noac042

11. Pandey R, Caflisch L, Lodi A, Brenner AJ, Tiziani S. Metabolomic signature of brain cancer. *Mol Carcinog*. Nov 2017;56(11):2355-2371. doi:10.1002/mc.22694

12. Chen J, Lee H, Schmitt P, et al. Bioengineered Models to Study Microenvironmental Regulation of Glioblastoma Metabolism. *J Neuropathol Exp Neurol*. Nov 19 2021;80(11):1012-1023. doi:10.1093/jnen/nlab092

13. Aftab K, Aamir FB, Mallick S, et al. Radiomics for precision medicine in glioblastoma. *J Neurooncol*. Jan 2022;156(2):217-231. doi:10.1007/s11060-021-03933-1

14. Jang K, Russo C, Di Ieva A. Radiomics in gliomas: clinical implications of computational modeling and fractal-based analysis. *Neuroradiology*. Jul 2020;62(7):771-790. doi:10.1007/s00234-020-02403-1

15. Moassefi M, Faghani S, Conte GM, et al. A deep learning model for discriminating true progression from pseudoprogression in glioblastoma patients. *J Neurooncol*. Sep 2022;159(2):447-455. doi:10.1007/s11060-022-04080-x

16. Hu LS, Hawkins-Daarud A, Wang L, Li J, Swanson KR. Imaging of intratumoral heterogeneity in high-grade glioma. *Cancer Lett*. May 1 2020;477:97-106. doi:10.1016/j.canlet.2020.02.025

17. Gaw N, Hawkins-Daarud A, Hu LS, et al. Integration of machine learning and mechanistic models accurately predicts variation in cell density of glioblastoma using multiparametric MRI. *Sci Rep*. Jul 11 2019;9(1):10063. doi:10.1038/s41598-019-46296-4

18. Zegers CML, Posch J, Traverso A, et al. Current applications of deep-learning in neuro-oncological MRI. *Phys Med*. Mar 2021;83:161-173. doi:10.1016/j.ejmp.2021.03.003

19. Zlochower A, Chow DS, Chang P, Khatri D, Boockvar JA, Filippi CG. Deep Learning AI Applications in the Imaging of Glioma. *Top Magn Reson Imaging*. Apr 2020;29(2):115-0. doi:10.1097/RMR.0000000000000237

20. Zhao H, Wang S, Song C, Zha Y, Li L. The prognostic value of MGMT promoter status by pyrosequencing assay for glioblastoma patients' survival: a meta-analysis. *World J Surg Oncol*. Oct 12 2016;14(1):261. doi:10.1186/s12957-016-1012-4

21. Liu L, Gerson SL. Targeted modulation of MGMT: clinical implications. *Clin Cancer Res*. Jan 15 2006;12(2):328-31. doi:10.1158/1078-0432.CCR-05-2543

22. Esteller M, Garcia-Foncillas J, Andion E, et al. Inactivation of the DNA-repair gene MGMT and the clinical response of gliomas to alkylating agents. *N Engl J Med*. Nov 9 2000;343(19):1350-4. doi:10.1056/NEJM200011093431901

23. Tautenhahn R, Patti GJ, Rinehart D, Siuzdak G. XCMS Online: a web-based platform to process untargeted metabolomic data. *Anal Chem*. Jun 5 2012;84(11):5035-9. doi:10.1021/ac300698c

24. Wei X, Shi X, Kim S, et al. Data dependent peak model based spectrum deconvolution for analysis of high resolution LC-MS data. *Anal Chem*. Feb 18 2014;86(4):2156-65. doi:10.1021/ac403803a

25. Wei X, Sun W, Shi X, et al. MetSign: a computational platform for high-resolution mass spectrometry-based metabolomics. *Anal Chem*. Oct 15 2011;83(20):7668-75. doi:10.1021/ac2017025

26. Nam SL, de la Mata AP, Dias RP, Harynuk JJ. Towards Standardization of Data Normalization Strategies to Improve Urinary Metabolomics Studies by GC×GC-TOFMS. *Metabolites*. 2020;10(9):376.

27. Bararpour N, Gilardi F, Carmeli C, et al. DBnorm as an R package for the comparison and selection of appropriate statistical methods for batch effect correction in metabolomic studies. *Sci Rep*. Mar 11 2021;11(1):5657. doi:10.1038/s41598-021-84824-3

28. Chong J, Soufan O, Li C, et al. MetaboAnalyst 4.0: towards more transparent and integrative metabolomics analysis. *Nucleic Acids Res*. Jul 2 2018;46(W1):W486-W494. doi:10.1093/nar/gky310

29. Maus A, Peters GJ. Glutamate and α-ketoglutarate: key players in glioma metabolism. *Amino Acids*. 2017/01/01 2017;49(1):21-32. doi:10.1007/s00726-016-2342-9

30. Schousboe A, Scafidi S, Bak LK, Waagepetersen HS, McKenna MC. Glutamate metabolism in the brain focusing on astrocytes. *Adv Neurobiol*. 2014;11:13-30. doi:10.1007/978-3-319-08894-5_2

31. Obara-Michlewska M, Szeliga M. Targeting Glutamine Addiction in Gliomas. *Cancers (Basel)*. Jan 29 2020;12(2)doi:10.3390/cancers12020310

32. Ijare O, Baskin D, Pichumani K. CBMT-01. ALANINE FUELS ENERGY METABOLISM OF GLIOBLASTOMA CELLS. *Neuro-Oncology*. 2019;21(Supplement_6):vi32-vi33. doi:10.1093/neuonc/noz175.123

33. Bulik M, Jancalek R, Vanicek J, Skoch A, Mechl M. Potential of MR spectroscopy for assessment of glioma grading. *Clinical Neurology and Neurosurgery*. 2013/02/01/ 2013;115(2):146-153. doi:https://doi.org/10.1016/j.clineuro.2012.11.002

34. Leonardi R, Jackowski S. Biosynthesis of Pantothenic Acid and Coenzyme A. *EcoSal Plus*. Apr 2007;2(2)doi:10.1128/ecosalplus.3.6.3.4

35. Hayflick SJ. Defective pantothenate metabolism and neurodegeneration. *Biochem Soc Trans*. Aug 2014;42(4):1063-8. doi:10.1042/BST20140098

36. Sang C, Philbert SA, Hartland D, et al. Coenzyme A-Dependent Tricarboxylic Acid Cycle Enzymes Are Decreased in Alzheimer's Disease Consistent With Cerebral Pantothenate Deficiency. *Front Aging Neurosci*. 2022;14:893159. doi:10.3389/fnagi.2022.893159

37. Guzzo G, Sciacovelli M, Bernardi P, Rasola A. Inhibition of succinate dehydrogenase by the mitochondrial chaperone TRAP1 has anti-oxidant and anti-apoptotic effects on tumor cells. *Oncotarget*. Dec 15 2014;5(23):11897-908. doi:10.18632/oncotarget.2472

38. Deng Z, Gu Y, Hou X, et al. Association between uric acid, cancer incidence and mortality in patients with type 2 diabetes: Shanghai diabetes registry study. *Diabetes Metab Res Rev*. Mar 2016;32(3):325-32. doi:10.1002/dmrr.2724

39. Fricker RA, Green EL, Jenkins SI, Griffin SM. The Influence of Nicotinamide on Health and Disease in the Central Nervous System. *Int J Tryptophan Res*. 2018;11:1178646918776658. doi:10.1177/1178646918776658

40. Jung J, Kim LJ, Wang X, et al. Nicotinamide metabolism regulates glioblastoma stem cell maintenance. *JCI Insight*. May 18 2017;2(10)doi:10.1172/jci.insight.90019

41. Liu J, Tao X, Zhu Y, et al. NMNAT promotes glioma growth through regulating post-translational modifications of P53 to inhibit apoptosis. *Elife*. Dec 17 2021;10doi:10.7554/eLife.70046

42. van Horssen R, Willemse M, Haeger A, et al. Intracellular NAD(H) levels control motility and invasion of glioma cells. *Cell Mol Life Sci*. Jun 2013;70(12):2175-90. doi:10.1007/s00018-012-1249-1

43. Ito T, Sato T, Takanashi Y, et al. A single oral supplementation of nicotinamide within the daily tolerable upper level increases blood NAD levels in healthy subjects. *Translational Medicine of Aging*. 2021;5:43-51. doi:https://doi.org/10.1016/j.tma.2021.09.001

44. Shireman JM, Atashi F, Lee G, et al. De novo purine biosynthesis is a major driver of chemoresistance in glioblastoma. *Brain*. May 7 2021;144(4):1230-1246. doi:10.1093/brain/awab020

45. Wang X, Yang K, Xie Q, et al. Purine synthesis promotes maintenance of brain tumor initiating cells in glioma. *Nat Neurosci*. May 2017;20(5):661-673. doi:10.1038/nn.4537

46. Minata M, Audia A, Shi J, et al. Phenotypic Plasticity of Invasive Edge Glioma Stem-like Cells in Response to Ionizing Radiation. *Cell Rep*. Feb 12 2019;26(7):1893-1905 e7. doi:10.1016/j.celrep.2019.01.076

47. Leventoux N, Augustus M, Azar S, et al. Transformation Foci in IDH1-mutated Gliomas Show STAT3 Phosphorylation and Downregulate the Metabolic Enzyme ETNPPL, a Negative Regulator of Glioma Growth. *Sci Rep*. Mar 26 2020;10(1):5504. doi:10.1038/s41598-020-62145-1

48. Engel AL, Lorenz NI, Klann K, et al. Serine-dependent redox homeostasis regulates glioblastoma cell survival. *Br J Cancer*. Apr 2020;122(9):1391-1398. doi:10.1038/s41416-020-0794-x

49. Takano N, Sarfraz Y, Gilkes DM, et al. Decreased expression of cystathionine beta-synthase promotes glioma tumorigenesis. *Mol Cancer Res*. Oct 2014;12(10):1398-406. doi:10.1158/1541-7786.MCR-14-0184

50. De Witte O, Goldberg I, Wikler D, et al. Positron emission tomography with injection of methionine as a prognostic factor in glioma. *J Neurosurg*. Nov 2001;95(5):746-50. doi:10.3171/jns.2001.95.5.0746

51. Sinnaeve J, Mobley BC, Ihrie RA. Space Invaders: Brain Tumor Exploitation of the Stem Cell Niche. *Am J Pathol*. Jan 2018;188(1):29-38. doi:10.1016/j.ajpath.2017.08.029

52. Chen J, Kumar S. Biophysical Regulation of Cancer Stem/Initiating Cells: Implications for Disease Mechanisms and Translation. *Curr Opin Biomed Eng*. Mar 2017;1:87-95. doi:10.1016/j.cobme.2017.02.006

53. Zhu X, Xu T, Peng C, Wu S. Advances in MALDI Mass Spectrometry Imaging Single Cell and Tissues. *Front Chem*. 2021;9:782432. doi:10.3389/fchem.2021.782432

TABLES

Patient	Ethnicity	Age at tissue collection	WHO Grade	Histology	IDH1 mutation status	MGMT mutation status	Primary or Recurrent?	Therapies administered prior to tissue collection
1	White	29	2	Oligoastrocytoma	**Positive**	Negative	Recurrent	Temozolomide; Radiation to the brain
2	White	63	4	Glioblastoma	Negative	**Positive**	Recurrent	Temozolomide; Radiation to the brain
3	White	74	4	Glioblastoma	Negative	Negative	Primary	None
4	White	75	4	Glioblastoma	Negative	Negative	Primary	None
5	White	23	4	Glioblastoma	Negative	N/A	Recurrent	Temozolomide; Lomustine; Radiation to the brain
6	Black or African American	34	4	Glioblastoma	Negative	Negative	Recurrent	Temozolomide
7	White	32	4	Glioblastoma	Negative	**Positive**	Primary	None
8	White	61	4	Glioblastoma	Negative	Negative	Primary	None
9	White	53	4	Glioblastoma	Negative	**Positive**	Primary	None
10	White	67	4	Glioblastoma	Negative	**Positive**	Primary	None
11	White	29	2	Astrocytoma	**Positive**	Negative	Primary	None
12	White	32	4	Glioblastoma	**Positive**	N/A	Primary	None
13	White	22	2	Astrocytoma	**Positive**	N/A	Primary	None
14	White	34	2	Oligodendroglioma	**Positive**	N/A	Primary	None
15	White	55	4	Glioblastoma	Negative	**Positive**	Primary	None
16	White	61	4	Glioblastoma	Negative	Negative	Primary	None
17	White	65	4	Glioblastoma	Negative	Negative	Primary	None
18	White	78	4	Glioblastoma	Negative	Negative	Primary	None
19	White	60	4	Glioblastoma	Negative	Negative	Primary	None
20	Black or African American	63	4	Glioblastoma	Negative	**Positive**	Primary	None
21	Black or African American	58	4	Glioblastoma	Negative	Negative	Primary	None
22	White	47	3	Oligodendroglioma	**Positive**	N/A	Recurrent	Temozolomide
23	White	72	4	Glioblastoma	Negative	Negative	Primary	None
24	Black or African American	63	4	Glioblastoma	Negative	Negative	Primary	None
25	White	65	4	Glioblastoma	Negative	Negative	Primary	None
26	White	63	4	Glioblastoma	Negative	**Positive**	Primary	None
27	White	31	4	Glioblastoma	Negative	Negative	Primary	None

Table 1. Table of patient characteristics.

FIGURES

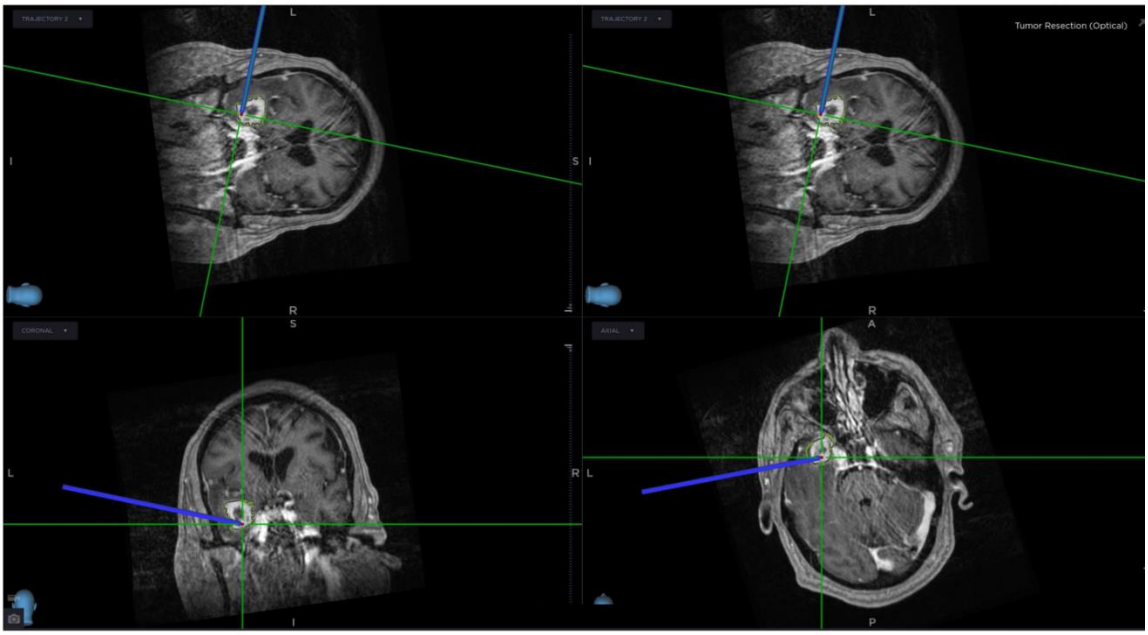

Figure_ 1. Intraoperative 3-dimensional navigation view using MRI imaging of a T1 post-contrast four panel views. Demonstrates representative core biopsy location within the contrast enhancing portion of the tumor.

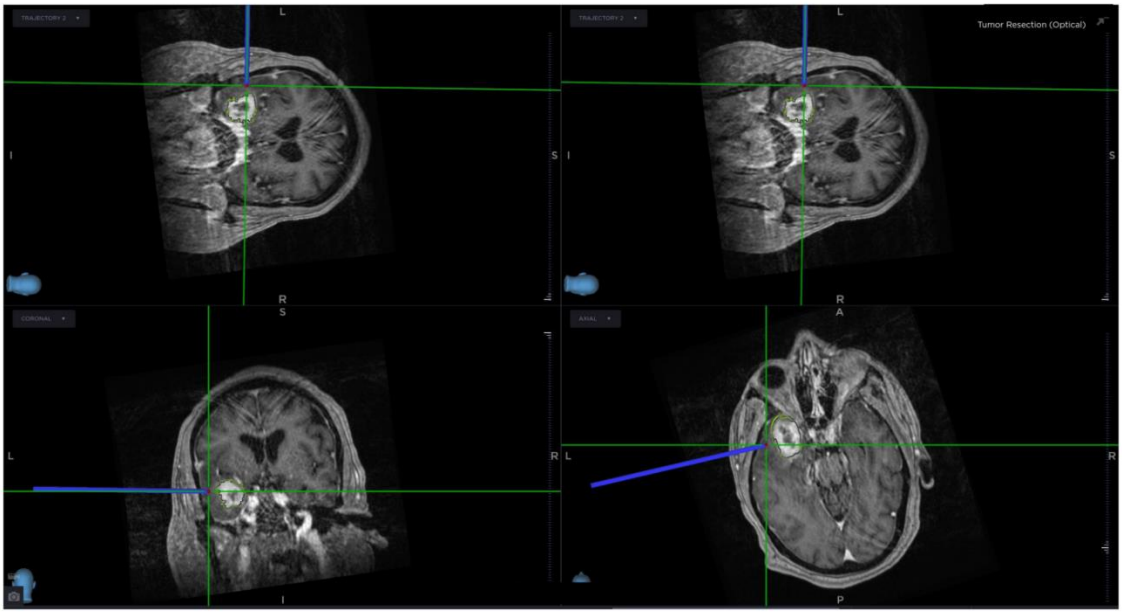

Figure_ 2. Intraoperative 3-dimensional navigation view using MRI imaging of a T1 post-contrast four panel views.

Demonstrates representative edge biopsy location outside the contrast enhancing portion of the tumor within the tumor infiltrating edge.

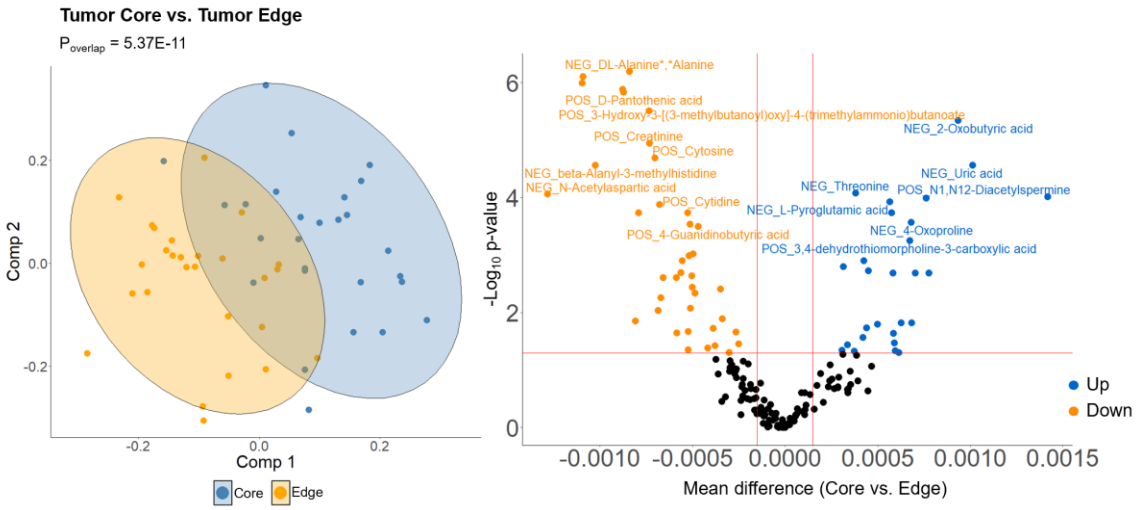

Figure_ 3. (Left) PLS-DA score plot of tumor core vs edge.

There was a significant separation between groups ($P_{overlap}$ = 5.37E-11) (Right) Volcano plot of significantly upregulated and downregulated metabolites of tumor core and tumor edge samples between patients, where tumor core is the reference. ‘POS’ and ‘NEG’ prefixes on metabolite names indicate whether the ion was detected in negative or positive ion mode. Blue points were increased in tumor core samples, and orange points were decreased in tumor core samples.

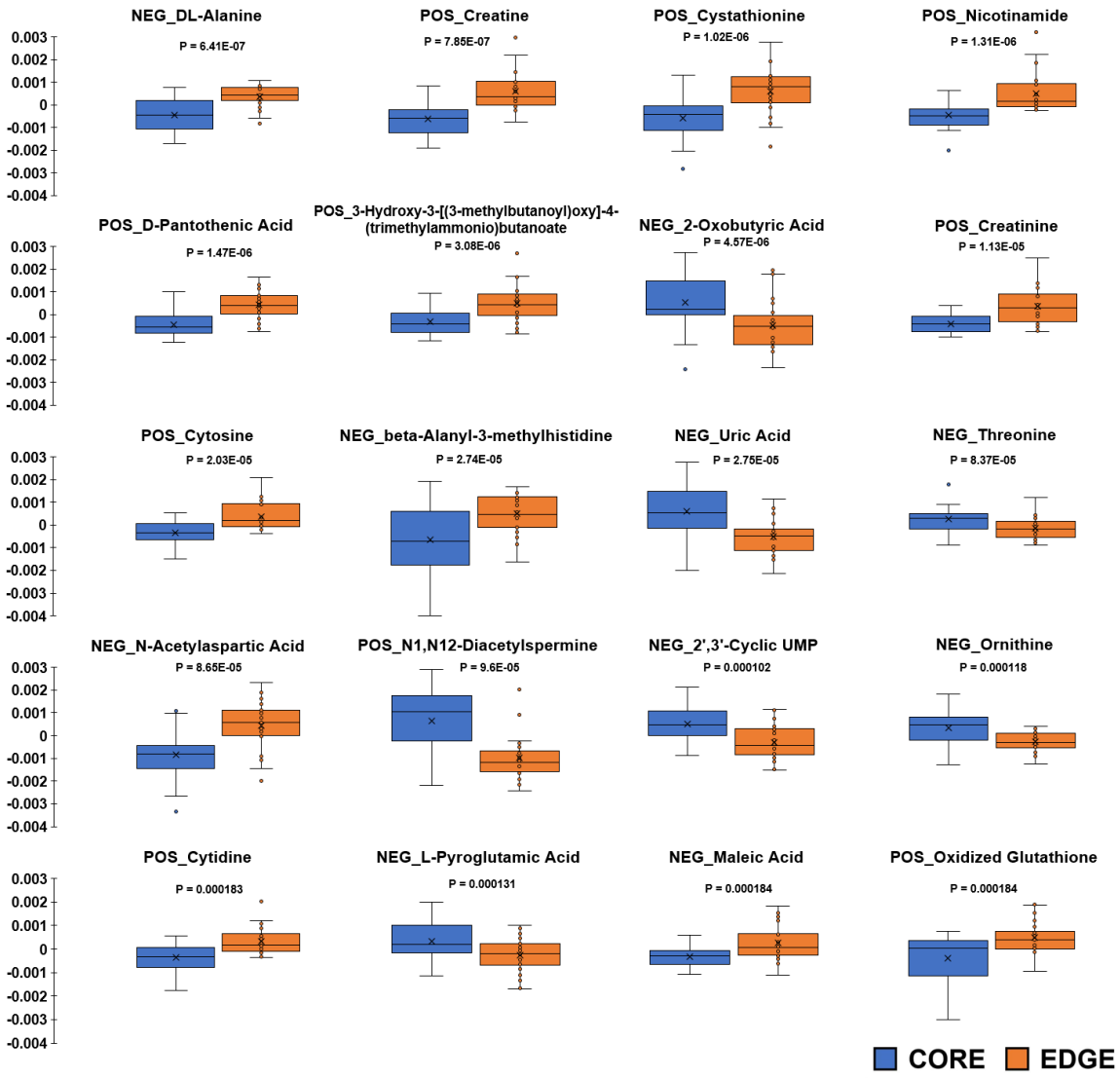

Figure_ 4. Relative abundance box plots of the top 20 metabolites differentiating between tumor core and tumor edge samples, ranked by p-value.

Paired t-tests or Wilcoxon rank sum tests were performed, depending on the normality of the data. ‘POS’ and ‘NEG’ prefixes on metabolite names indicate whether the ion was detected in negative or positive ion mode.

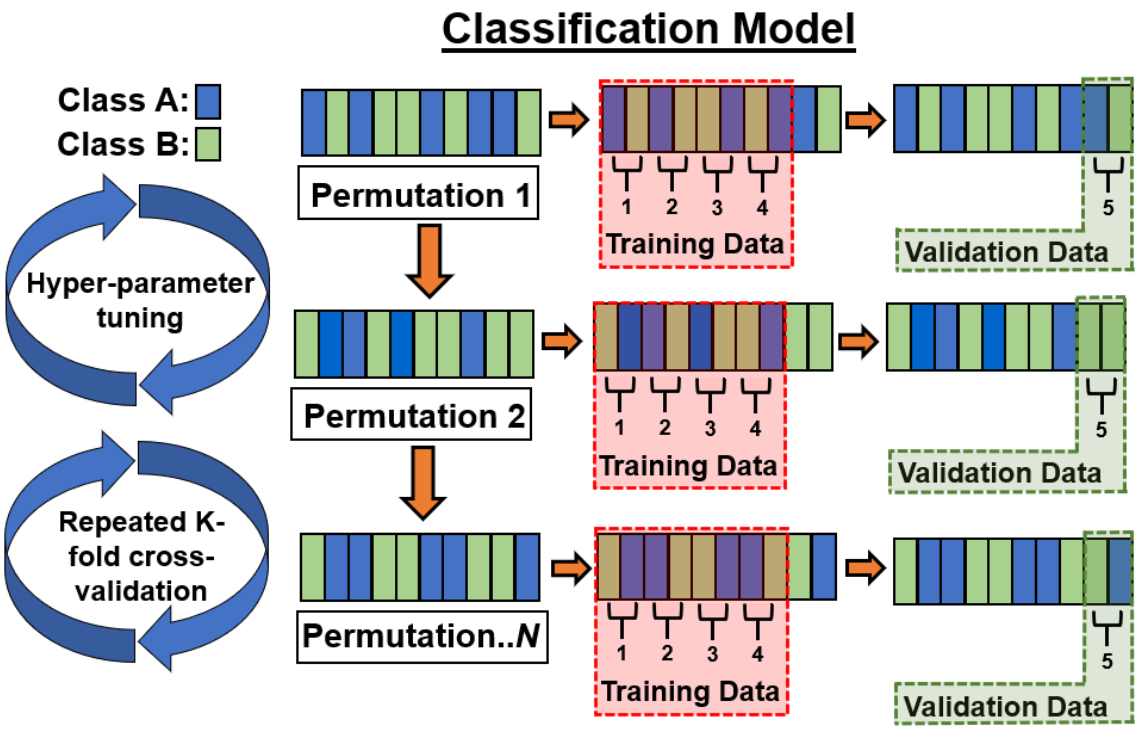

Figure_ 5. MGMT promoter methylation status, PLS-DA score plots, and classification model results.

Score plots indicate a significant separation between positive and negative MGMT promoter methylation groups with both (A) tumor core and (B) tumor edge metabolomic data. (C) A boosted generalized linear model (glmboost) was trained and validated with 5-fold cross validation using the top 4 metabolomic features as respectively ranked by variable importance for core and edge (Supplementary_Table_3), showing excellent classification performance with $AUROC_{Edge}$ = 0.960 (0.937 - 0.982) (95%CI) and $AUROC_{Core}$ = 0.941 (0.905 - 0.967) (95%CI). Dashed line represents a non-discriminatory reference model.

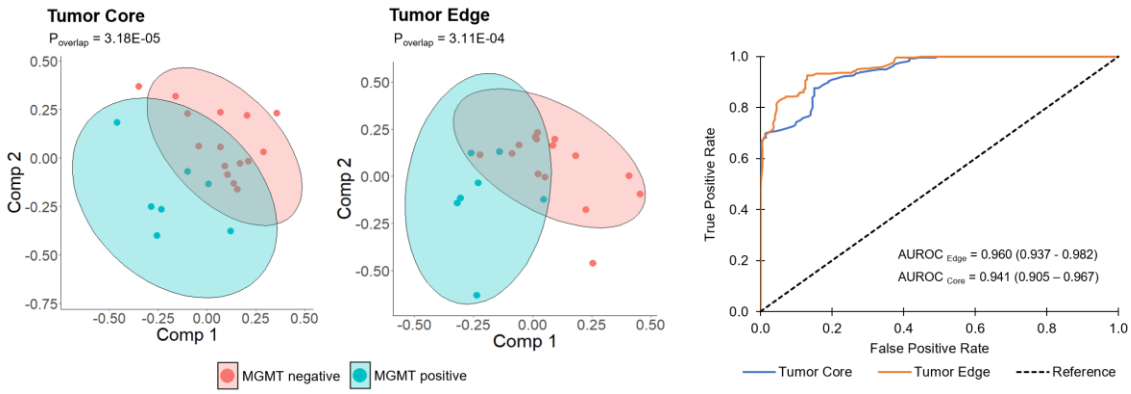

Figure_ 6. Machine learning model training and validation.

The permuted (randomly sorted) dataset is split into k folds (subsets; here, k=5). Model is trained with k-1 folds and validated with the kth fold. This process is repeated until all folds have been used once as the validation set. The next iteration of the cross validation involves another permutation of the complete dataset and repeating the whole process. Final results of each model are the averages of the validations across all folds and all iterations.

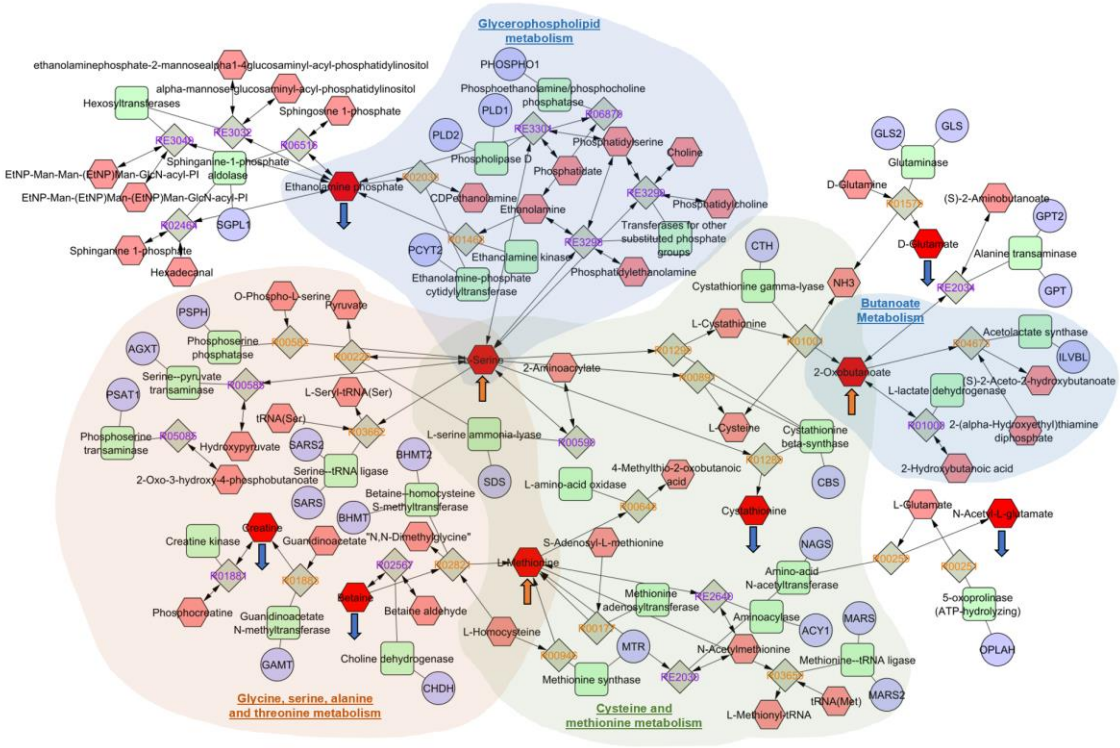

Figure_ 7. Pathway maps of significant metabolic pathways identified by QEA analysis for tumor core vs. edge, including glycerophospholipid metabolism, butanoate metabolism, cysteine and methionine metabolism, and glycine, serine, alanine and threonine metabolism.

Red source nodes are shown connected to compounds (pink hexagons), enzymes (green squares), genes (purple circles) and reactions (gray diamonds). Upward orange or downward blue arrows underneath each metabolite (red) node indicate if the metabolite was significantly upregulated or downregulated with respect to the tumor core. (e.g., creatine was downregulated in tumor core/upregulated in tumor edge; L-serine was upregulated in tumor core/downregulated in tumor edge).

APPENDIX

Metabolite	Core vs. Edge p-value
NEG_DL-Alanine	6.41E-07
POS_Creatine	7.86E-07
POS_Cystathionine	1.02E-06
POS_Nicotinamide	1.31E-06
POS_D-Pantothenic acid	1.47E-06
POS_3-Hydroxy-3-[(3-methylbutanoyl)oxy]-4-(trimethylammonio)butanoate	3.08E-06
NEG_2-Oxobutyric acid	4.57E-06
POS_Creatinine	1.14E-05
POS_Cytosine	2.04E-05
NEG_beta-Alanyl-3-methylhistidine	2.74E-05
NEG_Uric acid	2.75E-05
NEG_Threonine	8.37E-05
NEG_N-Acetylaspartic acid	8.65E-05
POS_N1,N12-Diacetylspermine	9.60E-05
NEG_2',3'-Cyclic UMP	1.02E-04
NEG_Ornithine	1.18E-04
POS_Cytidine	1.31E-04
NEG_L-Pyroglutamic acid	1.83E-04
POS_Oxidized glutathione	1.84E-04
NEG_Maleic acid	1.84E-04
NEG_4-Oxoproline	2.71E-04
POS_Glutaryl-L-carnitine	2.88E-04
POS_4-Guanidinobutyric acid	3.18E-04
POS_3,4-dehydrothiomorpholine-3-carboxylic acid	5.61E-04
POS_Hercynine	9.59E-04
POS_Hypoxanthine	1.02E-03
NEG_Methionine	1.25E-03
NEG_Glutamic acid	1.25E-03
NEG_Serine	1.59E-03
NEG_Leucine	1.86E-03
NEG_3-Hydroxy-3-methylglutaric acid	2.02E-03
NEG_Glutaric acid	2.05E-03
NEG_Citramalic acid	2.05E-03
POS_Palmitoylcarnitine	2.07E-03
POS_3-hydroxybutyrylcarnitine	2.30E-03
POS_S-(2-Hydroxyethyl)glutathione	2.47E-03
POS_Betain	2.47E-03
NEG_Pantothenic acid	3.65E-03
POS_1-Methyl-L-histidine	3.90E-03
POS_phosphoethanolamine	4.61E-03
POS_gamma-Amino-n-butyric acid	5.47E-03
POS_meglumine	8.46E-03
NEG_lysophosphatidylethanolamine (22:6(4Z,7Z,10Z,13Z,16Z,19Z)/0:0)	9.26E-03
NEG_Succinic anhydride	1.27E-02
NEG_L-Glutathione (reduced)	1.40E-02
NEG_2-Phosphoglycerate	1.51E-02
NEG_Pyrophosphoric Acid	1.51E-02
NEG_Glucosylgalactosyl hydroxylysine	1.58E-02
POS_Decanoylcarnitine	1.86E-02
NEG_Aspartic acid	1.87E-02
NEG_N-Acetyl-L-glutamic acid	2.14E-02
POS_Acetyl-L-carnitine	2.17E-02
NEG_Guanosine monophosphate	2.24E-02
NEG_Hippuric acid	2.30E-02
POS_N-Oleoyl-L-Serine	2.72E-02
NEG_Benzoic acid	3.40E-02
POS_N~6~,N~6~-Dimethyllysine	3.48E-02
NEG_Tyrosine	3.62E-02
POS_N6-METHYLLYSINE	3.74E-02
POS_Y-L-Glutamyl-L-glutamic acid	4.10E-02
NEG_3-AMP	4.42E-02
NEG_DL-p-Hydroxyphenyllactic acid	4.54E-02
NEG_diacetyl trimer	4.63E-02
NEG_5-CMP	4.65E-02
POS_1-[(1Z)-octadec-1-enyl]-sn-glycero-3-phosphoethanolamine	4.91E-02
POS_Butyryl-L-homoserine lactone	4.91E-02

Supplementary Table 1. P-values of metabolites with significant differences in relative abundance between paired tumor core and edge samples. ‘POS’ and ‘NEG’ prefixes on metabolite names indicate whether the ion was detected in negative or positive ion mode.

Tumor Core

Metabolite	MGMT status p-value
POS_Hydroxyhexanoycarnitine	2.38E-02
POS_Spermine	2.62E-02
POS_Proline	2.93E-02
POS_1-tetradecanoyl-2-[(9Z)-octadecenoyl]-sn-glycero-3-phosphocholine	3.87E-02
POS_Ethyl cinnamate	4.26E-02

Tumor Edge

Metabolite	MGMT status p-value
NEG_Itaconic acid	1.08E-02
NEG_Pantothenic acid	1.15E-02
NEG_Camphoric acid	3.19E-02
NEG_Guanosine	3.29E-02
POS_Camphor	4.65E-02

Supplementary Table 2. P-values of metabolites with significant differences in relative abundance between patients with MGMT positive or negative promoter methylation status using either tumor core or tumor edge samples. 'POS' and 'NEG' prefixes on metabolite names indicate whether the ion was detected in negative or positive ion mode.

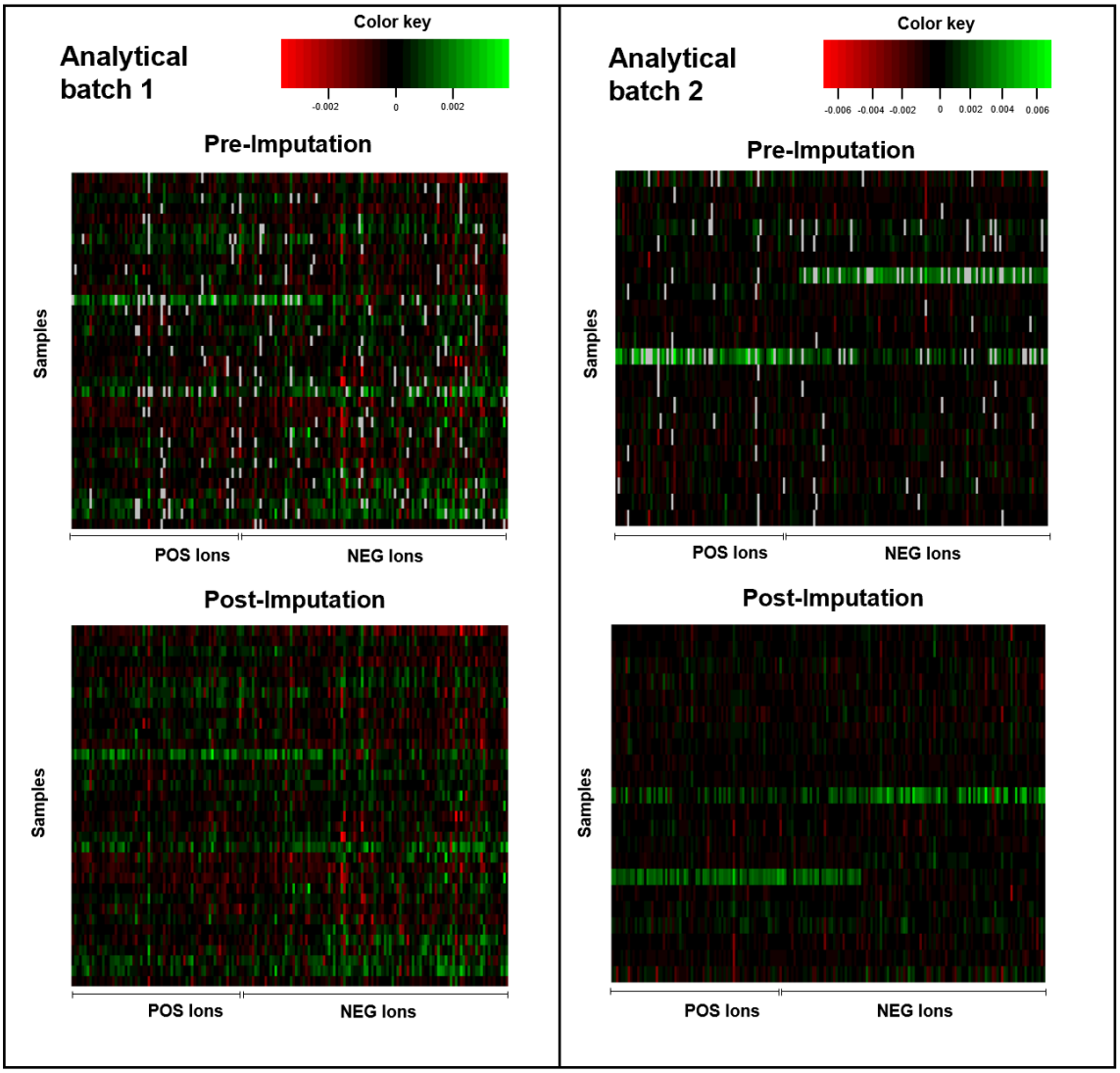

Supplementary Figure 1. Visualization of metabolomics data set before and after imputation. Log transformation, MSTUS normalization and centering have been performed prior to imputation. Red indicates low values and green high values of relative abundance. Gray indicates missing values, i.e. no signal was detected.

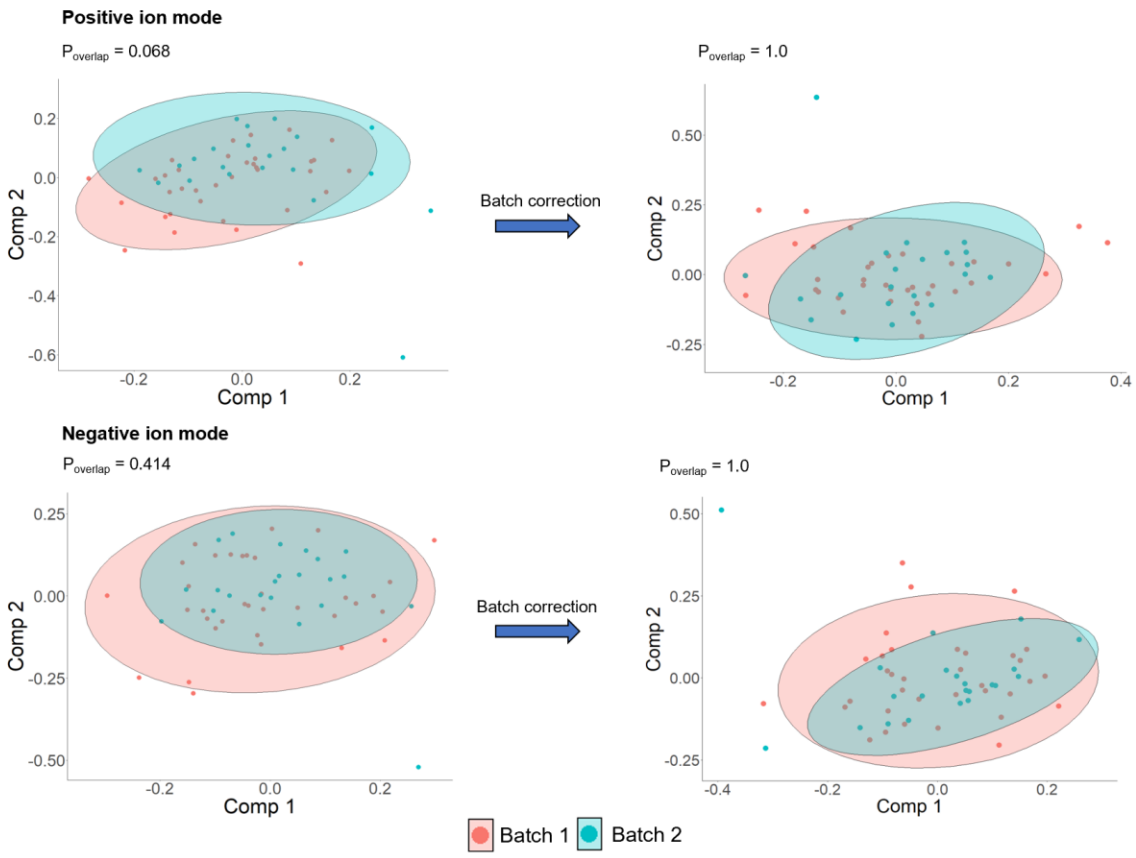

Supplementary Figure 2. PLS-DA score plots of analytical batch 1 and analytical batch 2 before and after batch correction. Separation between groups was decreased after batch correction.

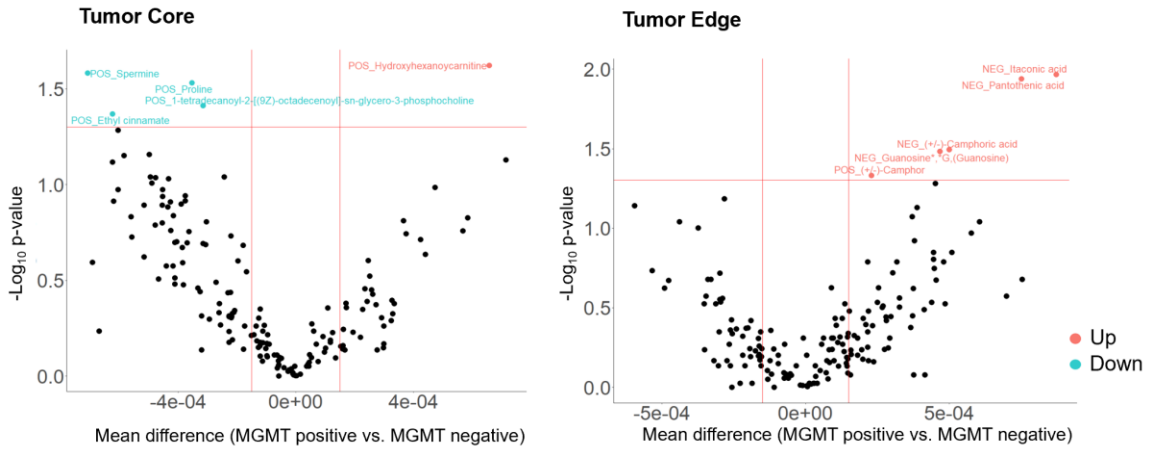

Supplementary Figure 3. Volcano plots of significantly upregulated and downregulated metabolites between patients with positive or negative MGMT promoter methylation status from the tumor core samples (left) and tumor edge samples (right), where negative MGMT status is the reference. Rose color points increased in negative MGMT samples, and teal colored points decreased in negative MGMT samples. 'POS' and 'NEG' prefixes on metabolite names indicate whether the ion was detected in negative or positive ion mode.

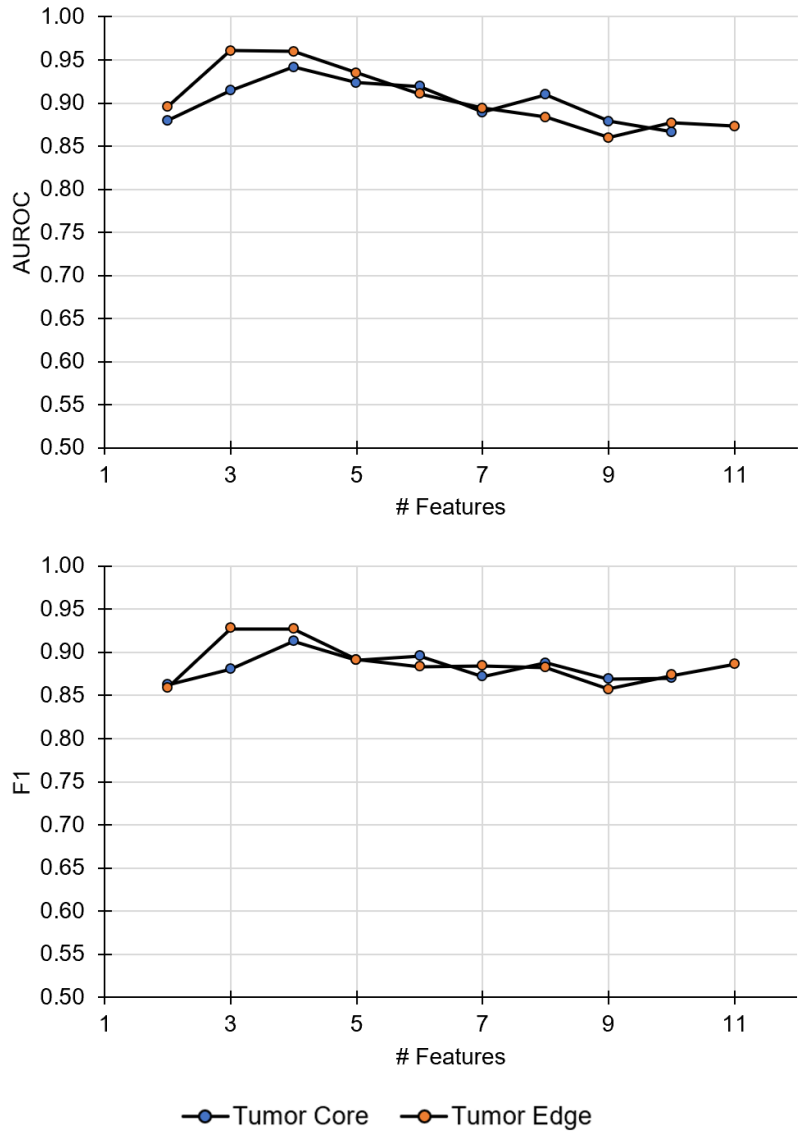

Supplementary Figure 4. AUROC and F1 of glmboost classification models during feature selection. Only features with non-zero variable importance were included during feature selection.

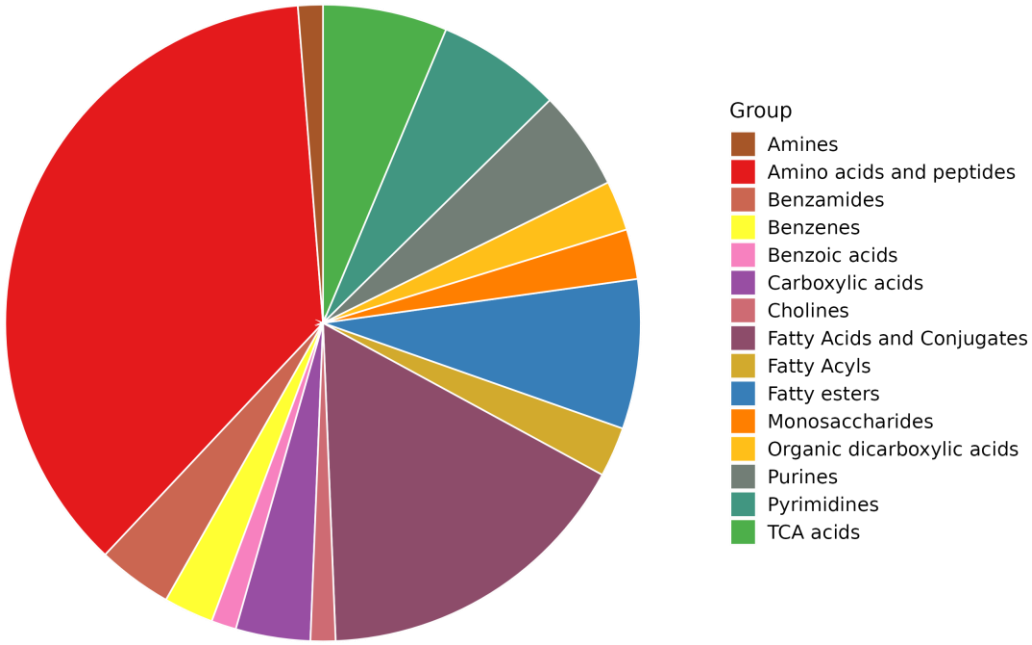

Supplementary Figure 5. Relative proportion of chemical structure main classes within tumor core and tumor edge samples across both analytical batches, produced by MetaboAnalyst 5.0.

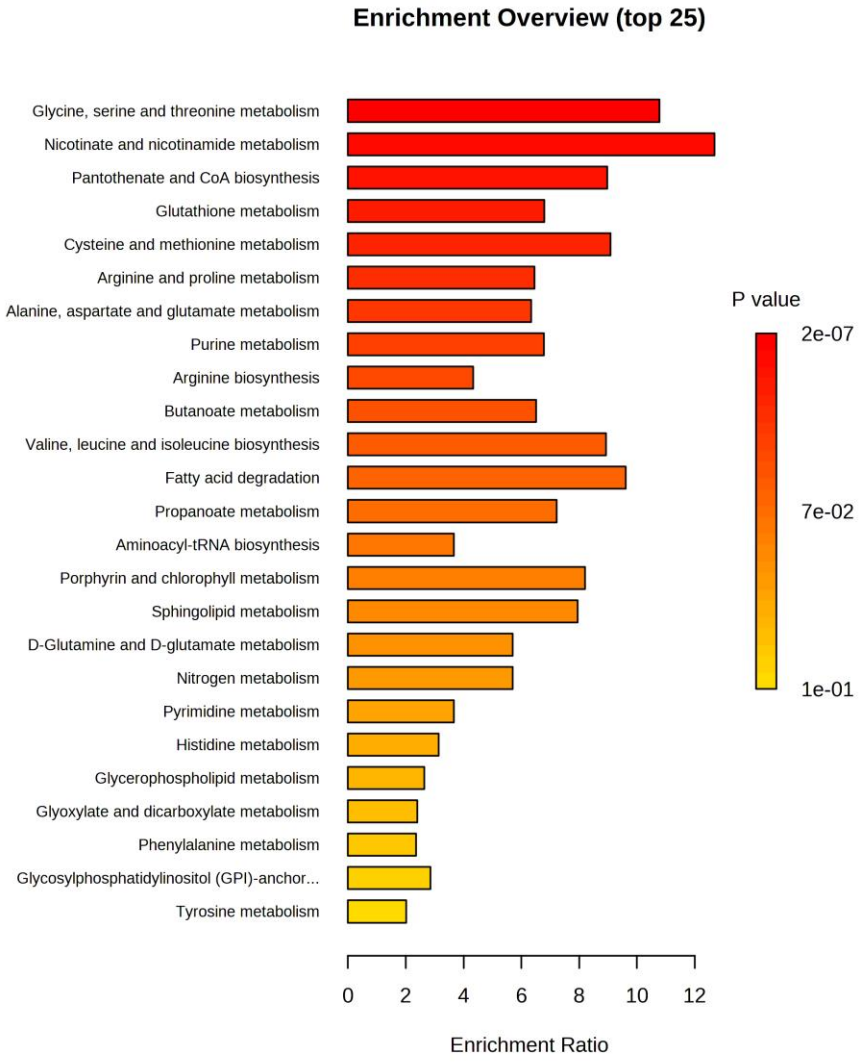

Supplementary Figure 6. Quantitative enrichment analysis of tumor core vs. tumor edge found with MetaboAnalyst 5.0 using the KEGG pathway database.

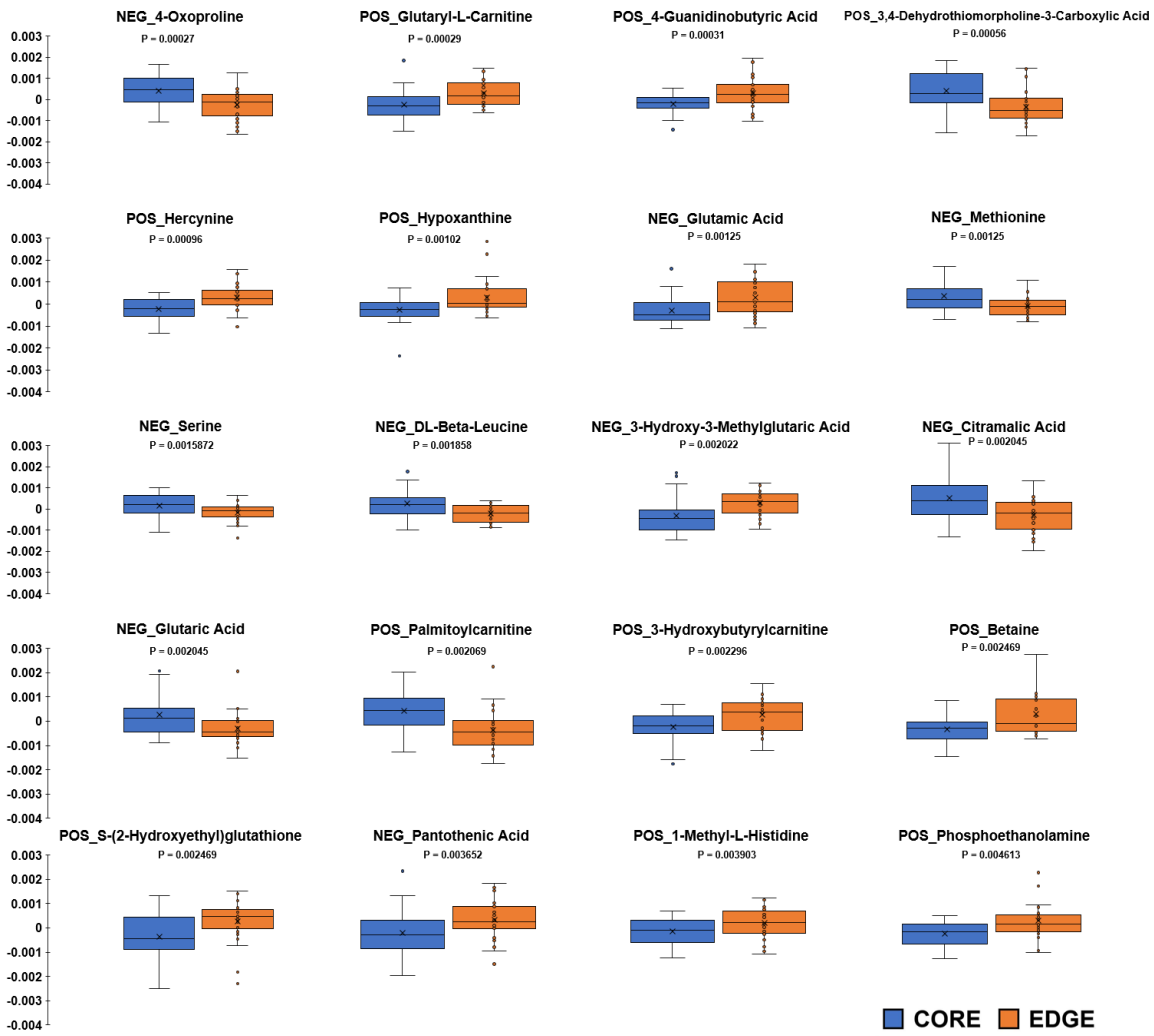

Supplementary Figure 7. Relative abundance box plots of the 20-40 top key metabolite differentiating tumor core and tumor edge samples. Paired t-tests or Wilcoxon rank sum tests were performed, depending on the normality of the data.

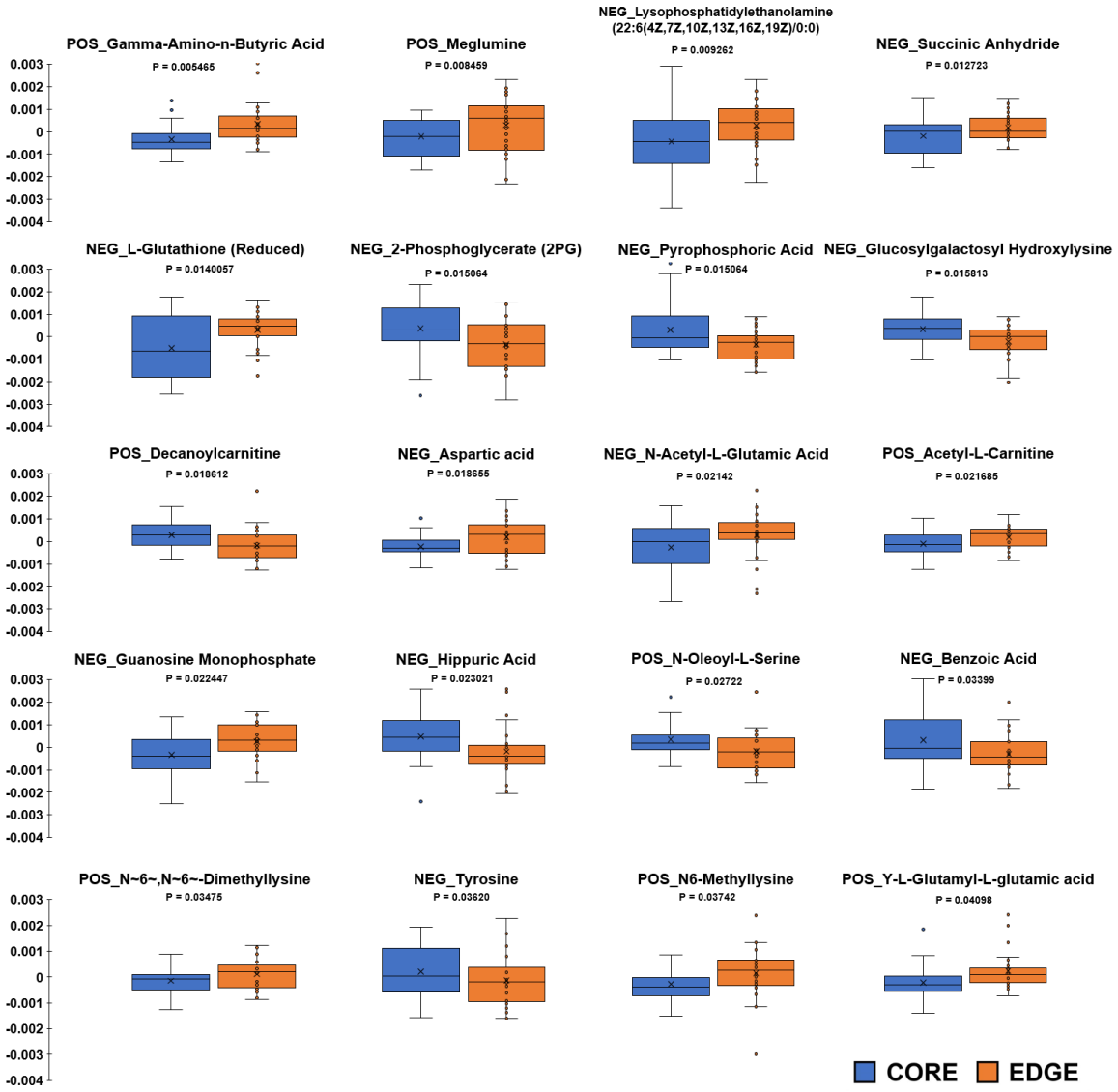

Supplementary Figure 8. Relative abundance box plots of the 40-60 top key metabolite differentiating tumor core and tumor edge samples. Paired t-tests or Wilcoxon rank sum tests were performed, depending on the normality of the data.

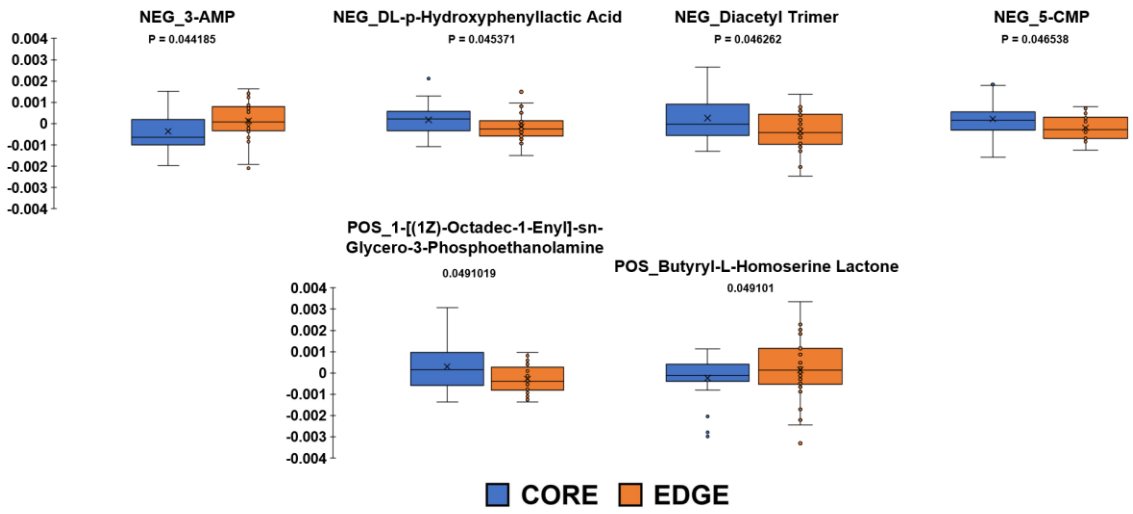

Supplementary Figure 9. Relative abundance box plots of the 61-66 top key metabolite differentiating tumor core and tumor edge samples. Paired t-tests or Wilcoxon rank sum tests were performed, depending on the normality of the data.

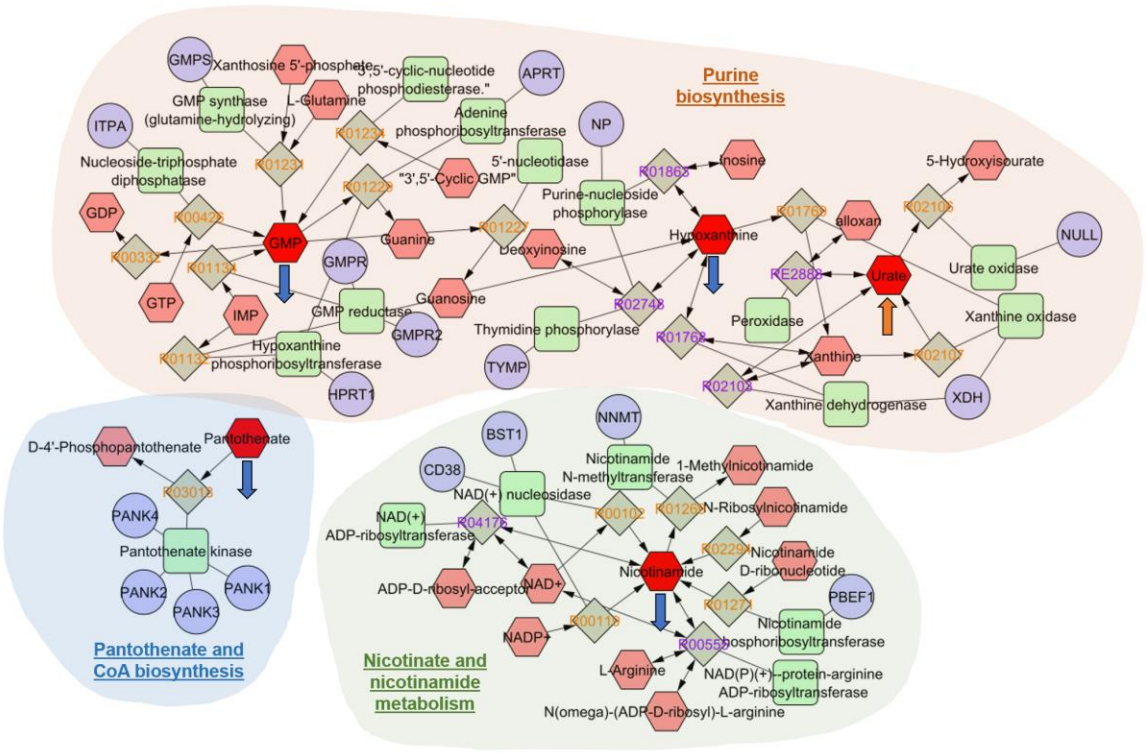

Supplementary Figure 10. Additional pathway maps of significant metabolic pathways identified by QEA analysis for tumor core vs. edge, including purine biosynthesis, pantothenate and CoA biosynthesis, and nicotinate and nicotinamide metabolism. Red source nodes are shown connected to compounds (pink hexagons), enzymes (green squares), genes (purple circles) and reactions (gray diamonds). Upward orange or downward blue arrows underneath each metabolite (red) node indicate if the metabolite was significantly upregulated or downregulated with respect to the tumor core. (e.g. pantothenate was downregulated in tumor core/upregulated in tumor edge; urate (i.e. uric acid) was upregulated in tumor core/downregulated in tumor edge).

CURRICULUM VITA

NAME:	Mary Elizabeth Baxter
ADDRESS:	132 Eastern Parkway Louisville, KY 40292 University of Louisville J.B. Speed School of Engineering
DOB:	Louisville, Kentucky – March 7th, 2000
EDUCATION & TRAINING:	B.S., Bioengineering University of Louisville 2018-2022
AWARDS:	Research! Louisville 1st Place Master of Engineering Category 2022 Mickey R. Wilhelm Achievement Award University of Louisville 2022 Biomedical Engineering Society Chapter Award University of Louisville 2022 Kentucky Association for Medical Instrumentation Student Essay Winner 2019
PROFESSIONAL SOCIETIES:	Biomedical Engineering Society 2018-2023 Tau Beta Pi 2022-∞ Phi Delta Epsilon 2019-2022

	University of Louisville Honors Program 2018-2022 Kentucky Association for Medical Instrumentation 2019-2021
PUBLICATIONS:	**1.** **Baxter, M., & Miller, H. et al.,** *Metabolomic differentiation of tumor core versus edge in glioma via machine learning.* Journal of Neurosurgery. Accepted for publication. In Press. 2. Kablan, R., & Miller, H. et al., *Evaluation of stacked ensemble model performance to predict clinical outcomes: a COVID-19 study*. In Review. 3. Centner, C., et al., *Modulation of acoustofluidic parameters to assess effect on molecular loading in human T cells.* The journal of the Acoustical Society of America, 2021. **150**(4). 4. Centner, C.S., et al., *Acoustofluidic-mediated molecular delivery to human T cells with a three-dimensional-printed flow chamber.* The Journal of the Acoustical Society of America, 2021. **150**(6): p. 4534-4547. 5. Centner, C.S., et al., *Comparison of Acoustofluidic and Static Systems for Ultrasound-Mediated Molecular Delivery to T Lymphocytes.* Ultrasound in Medicine & Biology, 2023. **49**(1): p. 90-105.
PRESENTATIONS:	Research! Louisville Abstract Presentation 2022